FORWARD-LOOKING IMAGING OF SCANNING PHASED ARRAY RADAR BASED ON THE COMPRESSED SENSING

Xiaoyang Wen[*], Gangyao Kuang, Jiemin Hu, Ronghui Zhan, and Jun Zhang

College of Electronic Science and Engineering, National University of Defense Technology, Changsha 410073, P. R. China

Abstract—In this paper, a novel forward-looking imaging method based on the compressed sensing is proposed for scanning phased array radar (PAR) in order to improve the azimuth resolution. Firstly, the echo of targets is modeled according to the principle of PAR. Then, it is analyzed why some of the former methods as multi-channel deconvolution are ineffective based on the signal model. Using a widely accepted assumption that dominant scatterers in an interesting area are sparse or compressible, an imaging algorithm based on the compressed sensing is proposed and investigated. This method obtains its high range resolution by transmitting and compressing chirp pulse signal, and improves its azimuth resolution by utilizing the compressed sensing technique. The effectiveness of the proposed method is illustrated and analyzed with simulations data.

1. INTRODUCTION

Since synthetic aperture radar (SAR) has the characteristics of imaging an interesting area with high resolution in all weather conditions, it moves radar technology from crude detection and estimation to fine resolution imaging and feature extraction [1–5]. Nowadays, it has become an important detecting tool in the military reconnaissance and civil remote sensing fields and has been widely used on airborne or missile-borne platforms. However, due to the limitations of its principle, the conventional SAR can work well only when the radar is side looking or squint looking with a small squint angle. If the radar

works with a large enough squint angle even under the forward-looking condition, it cannot provide images with high azimuth resolution. So the conventional SAR cannot be applied in certain scenarios, such as aircraft landing, which require the radar to image a forward swath rather than a sideward swath like a vehicle's headlight [4, 6]. It means that the SAR exists an imaging blind zone which locates at the forward of the platform.

In order to overcome this problem, many methods have been proposed and these methods can be divided into two categories roughly. The first is that the platform maneuvers along a pre-designed trajectory and lets the target area locate at the obliquely forward of the platform. The radar illuminates the target area with a high squint angle and synthetic aperture processing can be used to image the area. This method avoids the forward looking imaging problem. However, it can reduce but cannot eliminate the imaging blind zone. Especially at the end of the trajectory, the problem still exists. And this method increases demands for maneuverability of the platform. The second category includes various systematic or numerical methods, which have been proposed to enable the radar to image the forward swath with an azimuth resolution to some extent. Commonly, these methods can be categorized into the following classes.

(1). Forward imaging SAR using a forward looking array as the sector imaging radar for enhanced vision (SIREV) which has been developed at the German Aerospace Center [7–15]. The problem of this approach is that it has so complicated a system that when a high azimuth resolution is required, there will be an expensive and large-scale transformation to the existing systems. Even so, according to SAR, its azimuth resolution is constrained by the length of the synthetic aperture, which is equal to the real aperture length of the array, so this method is only suitable for landing of airplanes on which a large scale antenna can be achieved, and unsuitable if the aperture is not large enough, such as a missile-borne radar.

(2). Monopulse forward imaging based on monopulse angle measurement. This method is investigated in many literatures [16, 17] and it has been used in some systems [18]. This method uses the advantage of monopulse angle measurement which has high precision, but it cannot distinguish scatterers in the same range resolution cell.

(3). Forward imaging based on the technology of direction of arrival (DOA) [19, 20]. If this method is used, multiple channels are required, and the scatterers' number must be smaller than the channels'. It can be acquired that more scatterers mean more channels and more complicated system. And more important is that high-volume data should be processed. If a broadband signal is used, the

impact of bandwidth should be considered, which makes the algorithm more complicated.

(4). Scanning radar forward-looking imaging based on deconvolution [21–23]. Research of this method can be traced back to 1980s, and a lot of papers have been presented. Recently, because of the increasingly urgent requirement for the forward-looking imaging, it attracts people's attention again. Because the antenna pattern is a low-pass system and the single-channel deconvolution in the frequency domain cannot work well in the singular region, a multi-channel devolution method [24] in the frequency domain is proposed, which utilizes the characteristic of monopulse radar which has a sum and a difference channel. This method also includes some modified forms, such as deconvolution in the time domain [25], least square estimation (LSE) [26, 27], et al. Limitations of these approaches are that the imaging result is sensitive to the signal-to-noise ratio (SNR) and what matters more is that absolution of the antenna pattern is used in the former researches. But according to antenna theory, it is not the fact. If the phase of the antenna pattern is considered, its bandwidth in which area its spectrum is not equal to zero is finite and approximately equal to the electrical length of the antenna, so the azimuth resolution is approximately equal to the beam width of the antenna pattern, which will be investigated in detail in the paper. When deconvolution in time domain or LSE is used, the difficulty will be encountered because the sensing matrix is of a great condition number even ill-conditioned. The rank of the measurement matrix is much smaller than the azimuth resolution cells' number, so the equations will have many solutions. If some regularization technologies are adopted, the rank of the measurement matrix will be increased and its singularity will be eliminated. However, the equations will be changed seriously and the correct solution cannot be obtained.

In addition, there are some other forward-looking imaging methods, such as scanned angle/time correlation (SATC) [28] and bistatic forward-looking SAR imaging [29–37]. The former is not given detailed in the literature, and an important precondition of this method which is difficult to achieve is that the antenna pattern should maintain a fixed phase relationship with the transmitted signal during the azimuth scanning process, and what is more important is that echoes from different directions do not satisfy the translation invariance, These problems constrain the use of the method for forward-looking imaging. The latter is a promising method for forward-looking imaging with high resolution, but the difficulty is the synchronization of the receiver and the transmitter.

Now, more and more phased array radar (PAR) systems are

used on airborne or missile-borne platform, and sometimes, because of the limitations of the platform size, data storage capacity and costs, multiple channels cannot be achieved and the sensor has only two channels — the sum and the difference channel, which is named as monopulse PAR, so in this paper, the forward-looking imaging of monopulse PAR is considered. Signal model of an azimuth-scanning PAR is established according to its principle. Limitations of deconvolution forward-looking imaging algorithm are investigated in detail through theoretical analysis and experiments. A novel forward-looking imaging method is proposed based on compressed sensing (CS), which obtains high range resolution by pulse compression of a broadband signal and azimuth discrimination in the same range resolution cell by an optimum estimation based on CS for a sparse scene. After pulse compression, data of the same range cell at different azimuth scanning angles constitute the azimuth echo signal, and they are the sums of multiple targets' echoes from different azimuth directions which are weighted by the antenna pattern. Therefore, estimation of the targets' amplitudes and azimuths from the azimuth echo signal is an inverse problem. In most cases, inverse problems are underdetermined and ill-posed. And it is difficult to obtain an accurate and stable solution. Tikhonov regularization method [38, 39] can eliminate isolated singular points of the inverse problem. However, if the system function is equal to zero in a large continuous area of the frequency domain, such as an antenna pattern, it is difficult to get the correct answer. Compressed sensing can be used to resolve inverse problems [40], and it has been applied in radar imaging [41–44]. But it is mainly used to reduce the sampling pressure. If the sparsity of the scene is used as the regularization condition and CS is applied to forward-looking imaging, image resolution can be improved.

This paper is organized as follows. In Section 2, the signal model is established based on the principle of monopulse PAR. In Section 3, some deconvolution forward-looking imaging methods are analyzed in detail, which include the multi-channel deconvolution and the LSE method. The inefficiency of these methods is verified through theoretical analysis and simulations. Based on the prior information that the target area is sparse or compressible, a novel method based on compressed sensing is proposed, and performance of the method is established. In Section 4, some numerical simulation results are presented, and performance of the novel method is compared with the deconvolution imaging methods, and system parameters' impact also is analyzed.

2. ESTABLISHMENT OF THE SIGNAL MODEL

Suppose that the operating frequency is f_0 and corresponding wavelength λ_0. A forward-looking uniform linear PAR is constituted by M_x elements. The space between two adjacent elements is d_x. A chirp pulse is emitted during a single pulse repetition interval, its instantaneous bandwidth is B_r and its time duration is Γ. In order to simplify the problem, PAR remains stationary during an imaging period, thus impact of the motion can be ignored, and the chirp's bandwidth is so small that effects of aperture filled phenomenon can be ignored and azimuth scanning is achieved through phase-shifted method. Signals from the sum and the difference channels are obtained through weighting the signal from each element. The monopulse PAR's structure is shown in Fig. 1.
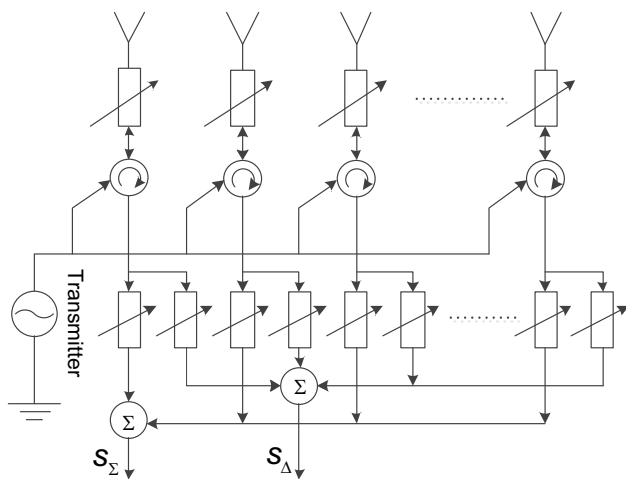

Figure 1. Structure diagram of a monopulse PAR.

Let the antenna phase center (APC) locate at the geometry center of the array. When the radar is working for forward-looking imaging, the beam of the antenna will scan the target area. If the beam's direction is θ_i^0, the signal emitted from the m_x-th element can be expressed as

$$s_{m_x}(i, t_f) = \text{rect}\left(\frac{t_f}{\Gamma}\right) \exp\left\{j2\pi f_0 t_f + j\pi\gamma t_f^2\right\} \exp\left\{-j2\pi f_0 \frac{m_x d_x \sin\theta_i^0}{c}\right\}$$

$$(1)$$

where i is the index number of a probe, and t_f is the fast time whose origin is located at the start of a pulse repeated interval as

many literatures have been explained about synthetic aperture radar. $\gamma = B_r/\Gamma$ is the chirp rate. If the k-th scatterer locates at (R_k, θ_k) and its amplitude is A_k, the distance between the scatter and the m_x-th element is equal to $R_{k,m_x} = R_k - m_x d_x \sin \theta_k$ approximately, where R_k is the distance between the scatterer and the APC, θ_k is its azimuth angle. Time delay between the scatterer and the element is $\tau_{k,m_x} = R_{k,m_x}/c = R_k/c - m_x d_x \sin \theta_k/c = \tau_k - \tau_{m_x}$, so the echo which is collected by the p-th element is given as follows

$$s_{k,p_x}(i, t_f) = A_k \exp\left\{-j2\pi f_0 \frac{p_x d_x \sin \theta_i^0}{c}\right\} \sum_{m_x} \exp\left\{-j2\pi f_0 \frac{m_x d_x \sin \theta_i^0}{c}\right\}$$

$$\text{rect}\left(\frac{t_f - \tau_{k,m_x} - \tau_{k,p_x}}{\Gamma}\right) \exp\left\{\begin{matrix} j2\pi f_0 \left(t_f - \tau_{k,m_x} - \tau_{k,p_x}\right) \\ +j\pi\gamma \left(t_f - \tau_{k,m_x} - \tau_{k,p_x}\right)^2 \end{matrix}\right\} \quad (2)$$

where $\tau_{p_x} = p_x d_x \sin \theta_k/c$, $\tau_{k,p_x} = R_{k,p_x}/c = R_k/c - p_x d_x \sin \theta_k/c = \tau_k - \tau_{p_x}$. In order to form the sum and difference antenna patterns with lower sidelobes, Taylor and Bayliss series are used to weight signals from these elements [45]. Supposing that the weighting series are $\mathbf{a}_\Sigma = [a_{\Sigma p_x}]$ and $\mathbf{a}_\Delta = [a_{\Delta p_x}]$ respectively, the signals which are collected by the radar are the weighted summation of the signal from each element and can be written as

$$s_{\Sigma k}(i, t_f) = \sum_{p_x} \{a_{\Sigma p_x} s_{k,p_x}(i, t_f)\} \quad (3)$$

$$s_{\Delta k}(i, t_f) = \sum_{p_x} \{a_{\Delta p_x} s_{k,p_x}(i, t_f)\} \quad (4)$$

If there are K scatterers in the target area, the signal can be expressed as

$$s_\Sigma(i, t_f) = \sum_k s_{\Sigma k}(i, t_f) \quad (5)$$

$$s_\Delta(i, t_f) = \sum_k s_{\Delta k}(i, t_f) \quad (6)$$

Based on the previous assumption, effects of the aperture filled phenomenon are ignored, and approximately, the signal from the sum channel can be rewritten as

$$s_\Sigma(i, t_f) \approx \sum_k A_k g_\Sigma\left(\theta_i^0, \theta_k\right) \text{rect}\left(\frac{t_f - 2\tau_k}{\Gamma}\right)$$

$$\exp\left\{j2\pi f_0(t_f - 2\tau_k) + j\pi\gamma(t_f - 2\tau_k)^2\right\} \quad (7)$$

where $g_\Sigma(\theta_i^0, \theta_k)$ is the gain of the sum channel antenna pattern which is given as

$$g_\Sigma\left(\theta_i^0, \theta_k\right)$$

$$= g_{\Sigma R}\left(\theta_i^0, \theta_k\right) g_T\left(\theta_i^0, \theta_k\right) = \sum_{p_x} a_{\Sigma p_x} \exp\left\{j2\pi f_0 \frac{p_x d_x\left(\sin\theta_k - \sin\theta_i^0\right)}{c}\right\}$$

$$\sum_{m_x} \exp\left\{j2\pi f_0 \frac{m_x d_x\left(\sin\theta_k - \sin\theta_i^0\right)}{c}\right\} \qquad (8)$$

Similarly, the signal from the difference channel can be expressed as

$$s_\Delta\left(i, t_f\right) \approx \sum_k A_k g_\Delta\left(\theta_i^0, \theta_k\right) \text{rect}\left(\frac{t_f - 2\tau_k}{\Gamma}\right)$$

$$\exp\left\{j2\pi f_0\left(t_f - 2\tau_k\right) + j\pi\gamma\left(t_f - 2\tau_k\right)^2\right\} \qquad (9)$$

where $g_\Delta(\theta_i^0, \theta_k)$ is the gain of the difference channel antenna pattern which is given as

$$g_\Delta\left(\theta_i^0, \theta_k\right)$$

$$= g_{\Delta R}\left(\theta_i^0, \theta_k\right) g_T\left(\theta_i^0, \theta_k\right) = \sum_{p_x} a_{\Delta p_x} \exp\left\{j2\pi f_0 \frac{p_x d_x\left(\sin\theta_k - \sin\theta_i^0\right)}{c}\right\}$$

$$\sum_{m_x} \exp\left\{j2\pi f_0 \frac{m_x d_x\left(\sin\theta_k - \sin\theta_i^0\right)}{c}\right\} \qquad (10)$$

Since signal processing of the sum and the difference channel are the same, only processing of the sum channel is given below. After down-conversion and pulse compression, the signal of the sum channel can be expressed as

$$s_\Sigma(i, t_f) \approx \sum_k A_k \exp\left\{-j4\pi f_0\tau_k\right\} \text{sinc}\left\{B_r\left(t_f - 2\tau_k\right)\right\} g_\Sigma\left(\theta_i^0, \theta_k\right) \quad (11)$$

Then azimuth resolution is obtained through processing the signal in the same range resolution cell which is formed by multiple probes. Herein, the number of probes is I. The echo collection model is illustrated in Fig. 2.

The length of the antenna pattern is defined as the region in which the gain is significantly larger than zero, and here is $N = 2K+1$, which is shown in Fig. 2(a) as a bold solid line. Echo collection process is illustrated in Fig. 2(b). It shows that the scanning process is a one of weighted summation to the echoes from different targets in the same

range resolution cell. Thus, after pulse compression the total signal also can be expressed in matrix form as

$$\mathbf{S}_\Sigma = \mathbf{G}_\Sigma \mathbf{X} \tag{12}$$

If noise is considered, it can be rewritten as

$$\mathbf{S}_\Sigma = \mathbf{G}_\Sigma \mathbf{X} + \mathbf{W}_\Sigma \tag{13}$$

If sampling points' number along the fast time is L, dimension of $\mathbf{S}_\Sigma$ is $I \times L$. Each row is a high range resolution profile of each probe, and each column has the same radial distance and constitutes the echo of the ring. Rows' number of $\mathbf{G}_\Sigma$ is I, and the i-th row is the sampling of the antenna pattern of the i-th probe. It should be noted that the antenna pattern is changing with the beam's direction, which is different from mechanical rotating radar. Sampling range is from $\theta_0^0 - K\delta\theta$ to $\theta_{I-1}^0 + K\delta\theta$, which is the total antenna patterns coverage of the whole scanning process and the number of sampling points is Q. Here, sampling interval of the antenna pattern is assumed as $\delta\theta$. It should be noted that, the sampling interval of the antenna pattern is not necessarily equal to the step between two adjacent probes which is denoted as $\Delta\theta$. Thus, the i-th row of $\mathbf{G}_\Sigma$ can be written as a row vector $\mathbf{g}_{\Sigma i} = [g_\Sigma(\theta_i^0, \theta_q)]$, where θ_q is a sampling point in $[\theta_0^0 - K\delta\theta, \theta_{I-1}^0 + K\delta\theta]$, and the length of $\mathbf{g}_{\Sigma i}$ is Q. The rows' number of $\mathbf{X}$ is equal to Q, which corresponds to the length of $\mathbf{g}_{\Sigma i}$, and its columns' number is equal to L, which corresponds to the range sampling number. Expressions of $\mathbf{S}_\Sigma$, $\mathbf{G}_\Sigma$, $\mathbf{X}$ are given as follows

$$\mathbf{S}_\Sigma = \begin{bmatrix} s_\Sigma(0, t_{f,0}) & s_\Sigma(0, t_{f,1}) & \dots & s_\Sigma(0, t_{f,L-1}) \\ s_\Sigma(1, t_{f,0}) & s_\Sigma(1, t_{f,1}) & \dots & s_\Sigma(1, t_{f,L-1}) \\ \vdots & \vdots & \ddots & \vdots \\ s_\Sigma(I-1, t_{f,0}) & s_\Sigma(I-1, t_{f,1}) & \dots & s_\Sigma(I-1, t_{f,L-1}) \end{bmatrix}$$

$$\mathbf{G}_\Sigma = \begin{bmatrix} g_\Sigma(\theta_0^0, \theta_0) & g_\Sigma(\theta_0^0, \theta_1) & \dots & g_\Sigma(\theta_0^0, \theta_{Q-1}) \\ g_\Sigma(\theta_1^0, \theta_0) & g_\Sigma(\theta_1^0, \theta_1) & \dots & g_\Sigma(\theta_1^0, \theta_{Q-1}) \\ \vdots & \vdots & \ddots & \vdots \\ g_\Sigma(\theta_{I-1}^0, \theta_0) & g_\Sigma(\theta_{I-1}^0, \theta_1) & \dots & g_\Sigma(\theta_{I-1}^0, \theta_{Q-1}) \end{bmatrix}$$

$$\mathbf{X} = \begin{bmatrix} A(\theta_0, t_{f,0}) & A(\theta_0, t_{f,1}) & \dots & A(\theta_0, t_{f,L-1}) \\ A(\theta_1, t_{f,0}) & A(\theta_1, t_{f,1}) & \dots & A(\theta_1, t_{f,L-1}) \\ \vdots & \vdots & \ddots & \vdots \\ A(\theta_{Q-1}, t_{f,0}) & A(\theta_{Q-1}, t_{f,1}) & \dots & A(\theta_{Q-1}, t_{f,L-1}) \end{bmatrix}$$

where, $t_{f,l}$ $(l = 0, 1, \dots, L-1)$ is each sampling instant along the fast time, $A(\theta_q, t_{f,l})$ is the amplitude of the scatterer at $(\theta_q, ct_{f,l}/2)$
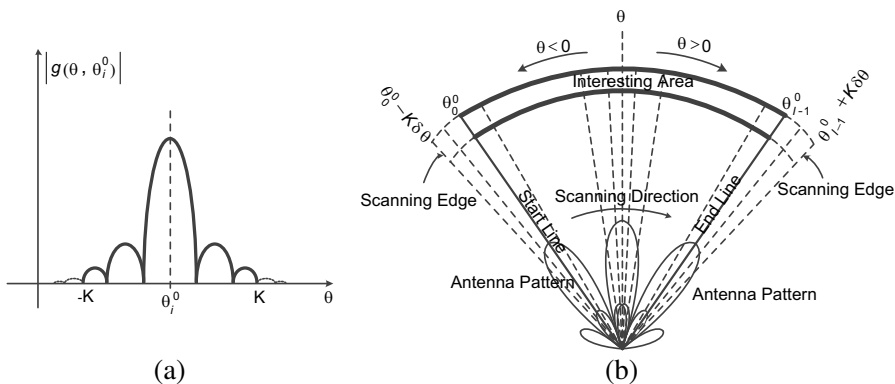
Figure 2. Signal received process. (a) Truncated antenna pattern. (b) Signal collection process of the scanning radar.

with the impact of the pulse compression, which contains a delayed phase determined by the radial distance. Obviously, it can be seen that $\mathbf{X}$ is a mesh dissection of the target area. In case that $\mathbf{X}$ could be recovered through signal processing, finer dissection means higher resolution. Because the antenna pattern has a certain beam width, beam coverage is larger than the scanning area, which is to say that the range from $\theta_0^0 - K\delta\theta$ to $\theta_{I-1}^0 + K\delta\theta$ is larger than that from θ_0^0 to θ_{I-1}^0, which is illustrated in Fig. 2(b), and commonly in order to improve the resolution, $\delta\theta$ is smaller than $\Delta\theta$, so $Q > I$, and it means that Equations (12) and (13) are underdetermined, and the number of unknowns is larger than the equations' number.

3. IMAGING ALGORITHM

If Equations (11), (12) and (13) can be solved, a high resolution image can be achieved. The antenna pattern of the PAR changes with the beam's direction which is different from the mechanical rotating radar, and from the point of signal and system, it means that the antenna pattern is a linear time-varying system. The azimuth echo is a result of the target area information passing through this linear time-varying system. We cannot use the linear deconvolution method to solve this problem. However, if the scanning range is small enough, the antenna pattern can be considered as a constant and approximately time-invariant system. Deconvolution in the frequency domain is highly time-efficient, which is benefit for achieving real-time implementation. If this algorithm could be used to obtain high azimuth

resolution, it was a promising method for forward-looking imaging, and performance of the scanning radar would be improved significantly. Because the antenna pattern of a single channel has singular areas, multi-channel deconvolution has been proposed. This method utilizes the characteristic that a monopulse radar has two channels, the sum and the difference channel. Unfortunately, it is inefficient for azimuth resolution improvement, which will be verified below. In addition, two channels can double the number of the equations while the number of unknowns keeps constant, so LSE has been proposed for solving equations. Some results of LES is presented, which shows that this is inefficient, and the reason is analyzed. Based on the analysis about the echo collected by the PAR, a novel forward-looking imaging method using compressed sensing is proposed.

3.1. Analysis of the Two-channel Deconvolution Forward-looking Imaging Method

For a scanning monopulse radar, the received echo can be modeled as

$$s_\Sigma(\theta, t_f) = x(\theta, t_f) \otimes g_\Sigma(-\theta) + w_\Sigma(\theta, t_f) \quad (14)$$

$$s_\Delta(\theta, t_f) = x(\theta, t_f) \otimes g_\Delta(-\theta) + w_\Delta(\theta, t_f) \quad (15)$$

where $x(\theta, t_f)$ is the targets' distribution on the ring distance from which to the APC is $ct_f/2$, $g_\Sigma(\theta)$ and $g_\Delta(\theta)$ are the sum and the difference channel antenna pattern respectively. $w_\Sigma(\theta, t_f)$ and $w_\Delta(\theta, t_f)$ are noise, and the symbol '$\otimes$' means the convolution of two functions. Result of two-channel deconvolution is given as

$$X(\Theta, t_f)$$
$$= \frac{G_\Sigma^*(-\Theta)S_\Sigma(\Theta, t_f)/W_\Sigma^2(\Theta, t_f) + G_\Delta^*(-\Theta)S_\Delta(\Theta, t_f)/W_\Delta^2(\Theta, t_f)}{G_\Sigma^*(-\Theta)G_\Sigma(-\Theta)/W_\Sigma^2(\Theta, t_f) + G_\Delta^*(-\Theta)G_\Delta(-\Theta)/W_\Delta^2(\Theta, t_f)} \quad (16)$$

If noise is not taken into account or the noise's spectrums of two channels are the same, Equation (16) can be rewritten as

$$X(\Theta, t_f) = \frac{G_\Sigma^*(-\Theta)S_\Sigma(\Theta, t_f) + G_\Delta^*(-\Theta)S_\Delta(\Theta, t_f)}{G_\Sigma^*(-\Theta)G_\Sigma(-\Theta) + G_\Delta^*(-\Theta)G_\Delta(-\Theta)} \quad (17)$$

where $X(\Theta, t_f)$, $S_\Sigma(\Theta, t_f)$, $S_\Delta(\Theta, t_f)$, $G_\Sigma(-\Theta)$, $G_\Delta(-\Theta)$ are the Fourier transformations of $x(\theta, t_f)$, $s_\Sigma(\theta, t_f)$, $s_\Delta(\theta, t_f)$, $g_\Sigma(-\theta)$ and $g_\Delta(-\theta)$ respectively. $W_\Sigma^2(\Theta, t_f)$ and $W_\Delta^2(\Theta, t_f)$ are the power spectral density functions of $w_\Sigma(\theta, t_f)$ and $w_\Delta(\theta, t_f)$ respectively. The superscript '*' means complex conjugate. The inverse Fourier transformation of $X(\Theta, t_f)$ is the scatterers' distribution. From the upper analysis, some conclusions can be obtained. Singular areas of $X(\Theta, t_f)$ are determined by $G_\Sigma(-\Theta)$ and $G_\Delta(-\Theta)$, i.e., zero points

of $G_{\Sigma}(\Theta)$ and $G_{\Delta}(\Theta)$. According to the principle of sum-difference amplitude-comparison monopulse technology, $g_{\Sigma}(\theta)$ and $g_{\Delta}(\theta)$ can be expressed as

$$g_{\Sigma}(\theta) = g(\theta - \Delta\theta) + g(\theta + \Delta\theta) \tag{18}$$
$$g_{\Delta}(\theta) = g(\theta - \Delta\theta) - g(\theta + \Delta\theta) \tag{19}$$

where $g(\theta - \Delta\theta)$ and $g(\theta + \Delta\theta)$ are two sub-beams' antenna patterns which are used to form the sum channel antenna pattern and the difference channel antenna pattern, respectively. $\Delta\theta$ is half of the angular interval between these two sub-beams. Fourier transformations of $g_{\Sigma}(\theta)$ and $g_{\Delta}(\theta)$ are given by

$$G_{\Sigma}(\Theta) = 2\cos(2\pi\Theta\Delta\theta)G(\Theta) \tag{20}$$
$$G_{\Delta}(\Theta) = -j2\sin(2\pi\Theta\Delta\theta)G(\Theta) \tag{21}$$

It shows that zero points of $G(\theta)$ also are zero points of $G_{\Sigma}(\Theta)$ and $G_{\Delta}(\Theta)$. If the antenna surface current intensity is $I(u)$ and the aperture length is L, the antenna pattern can be expressed as

$$g(\theta) = \int_{-L/2}^{L/2} I(u) \exp\left\{-j2\pi f_0 \frac{u\sin\theta}{c}\right\} du \tag{22}$$

Generally, L is much larger than $\lambda_0 = c/f_0$ and the beam is so narrow that Equation (22) can be approximated as follows

$$g(\theta) \approx \int_{-L/2}^{L/2} I(u) \exp\left\{-j2\pi f_0 \frac{u\theta}{c}\right\} du \tag{23}$$

So $G(\Theta)$ can be expressed as

$$G(\Theta) = \int_{-\pi}^{\pi} \int_{-L/2}^{L/2} I(u) \exp\left\{-j2\pi f_0 \frac{u\theta}{c}\right\} \exp\left\{-j2\pi\Theta\theta\right\} du d\theta$$
$$= I\left(-\frac{c\Theta}{f_0}\right) \tag{24}$$

Since $I(u)$ is non-zero only in $[-L/2, L/2]$, $G(\Theta)$ will be non-zero only under the condition that $|\Theta| \leq Lf_0/(2c)$, which means that the value of $X(\Theta, t_f)$ can be recovered only when it is in $[-Lf_0/(2c), Lf_0/(2c)]$, and the length of this area is $L/(c/f_0)$, so the azimuth resolution is $(c/f_0)/L$ which is equal to the beam width of one-way antenna pattern. Similarly, the azimuth resolution of the round-trip antenna pattern is $(c/f_0)/(2L)$ which is equal to the beam width

of the round-trip antenna pattern. Exact Fourier transformation of $g(\theta)$ can be expressed as

$$G(\Theta) = \int_{-\pi}^{\pi} g(\theta) \exp\{-j2\pi\Theta\theta\} \, d\theta$$

$$= 2\pi\lambda_0 \int_{-L/(2\lambda_0)}^{L/(2\lambda_0)} I(v) J_{2\pi\Theta}(-2\pi v) dv \qquad (25)$$

where $J_{2\pi\Theta}(-2\pi v)$ is the first kind Bessel function. It shows that, $G(\Theta)$ is a Bessel integral and it is difficult to obtain its accurate expression, but its change rule can be found by numerical analysis. The numerical integral of $G(\Theta)$ can be expressed as

$$G(\Theta) = 2\pi\lambda_0 \sum_{-L/(2\lambda_0)}^{L/(2\lambda_0)} I(v) J_{2\pi\Theta}(-2\pi v) \Delta v \qquad (26)$$

Suppose that the antenna current distribution is uniform and electrical length of the aperture L/λ_0 equal to 20, 40 or 80, which means $v = [-10, 10]$, $[-20, 20]$ or $[-40, 40]$, respectively. The numerical integral is illustrated in Fig. 3. It shows that, if Θ is larger than L/λ_0, the value of $G(\Theta)$ will decline to zero rapidly, so multi-channel deconvolution in the frequency domain cannot be used to the forward-looking imaging.

The function $|\text{sinc}(\cdot)|$ is often used as an approximation of the antenna pattern for forward-looking imaging in the existing literatures. An instance is given below. Supposing that every sub-beam's width is $4°$, and $2\Delta\theta = 0.4°$, rotating frequency of the antenna is 6 rounds per minute and the scanning area ranges from $-15°$ to $15°$. A chirp pulse is emitted in each pulse repeated interval, the operating frequency is $10\,\text{GHz}$, $B_r = 150\,\text{MHz}$, its pulse time duration is $5\,\mu\text{s}$ and the pulse repeated frequency is $1000\,\text{Hz}$. Distribution of the scatterers is illustrated in Fig. 4, and these amplitudes are all equal to 1. Imaging result with high resolution of multi-channel deconvolution is shown in Fig. 5(a). Every scatterer can be discriminated. However, if the function $\text{sinc}(\cdot)$ which is closer to the real situation is used, the imaging result is shown in Fig. 5(b). It shows that high azimuth resolution cannot be achieved. The reason is that $|\text{sinc}(\cdot)|$ has a wider and richer frequency domain information than $\text{sinc}(\cdot)$ and the bandwidth of $\text{sinc}(\cdot)$ is limited. However, it can be deduced from above analysis that $|\text{sinc}(\cdot)|$ cannot be realized.

Above theoretical analysis and simulations prove that multi-channel deconvolution cannot be used to improve azimuth resolution of
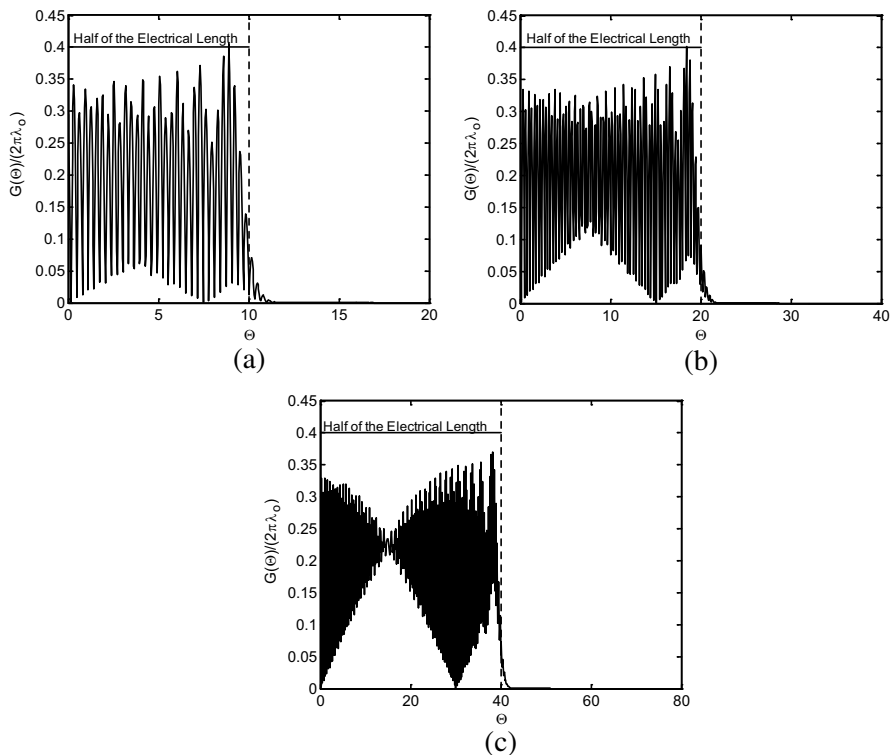
Figure 3. Bessel integration with different electrical length. (a) Electrical length equal to 20. (b) Electrical length equal to 40. (c) Electrical length equal to 80.
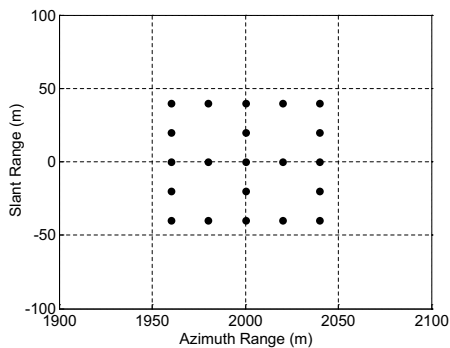

Figure 4. Distribution of the scatterers (illustrated as black dots).

the image formed by the antenna-rotating radar. In fact this derivation for phased array radar is also true. If scanning area is not large enough, the antenna pattern can be considered approximately as a constant.
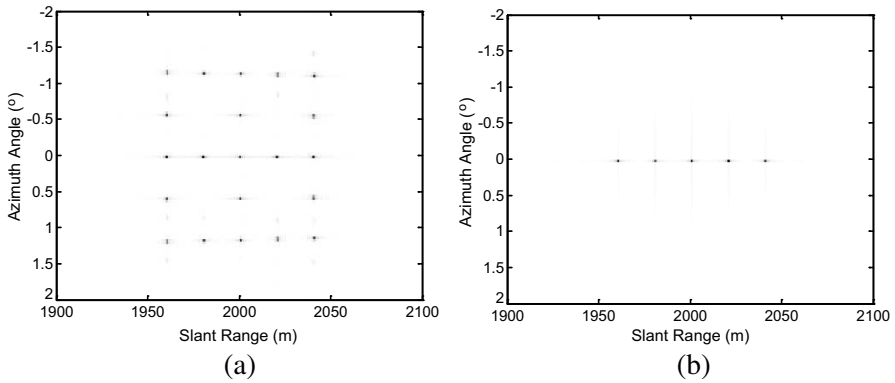
Figure 5. Imaging result using different antenna patterns. (a) Imaging result using the |sinc| antenna pattern. (b) Imaging result using the sinc antenna pattern.
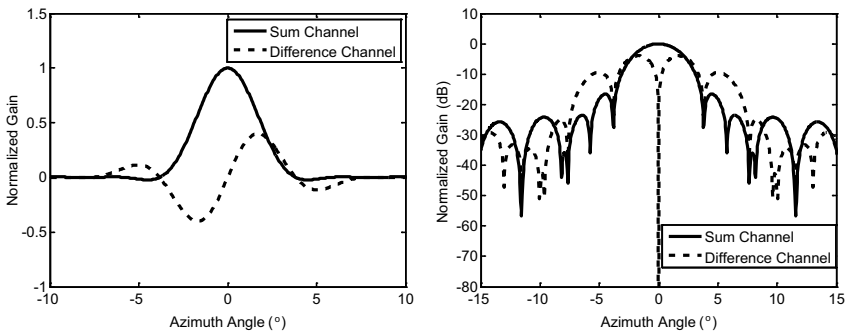

Figure 6. Antenna pattern of the monopulse phased array radar.

Although the principle of monopulse PAR has little difference with the monopulse mechanical rotating radar, the essence is the same, Fourier transformation of the PAR antenna pattern is also equal to the antenna current distribution density approximately, and its bandwidth also is determined by the electrical length of the aperture. For an instance, supposing that the operating frequency f_0 is $35\,\text{GHz}$ and that the number of elements is 25, the distance between two adjacent elements is 0.6 times of the wavelength λ_0; chirp signal is used, $B_r = 80\,\text{MHz}$, $\Gamma = 5\,\mu\text{s}$; scanning area ranges from $-15.6°$ to $15.6°$ with a constant step; Taylor and Bayliss series are used to form the sum and the difference channel antenna pattern, respectively. The antenna patterns are shown in Fig. 6 when the beams are pointing along the normal line of the array.

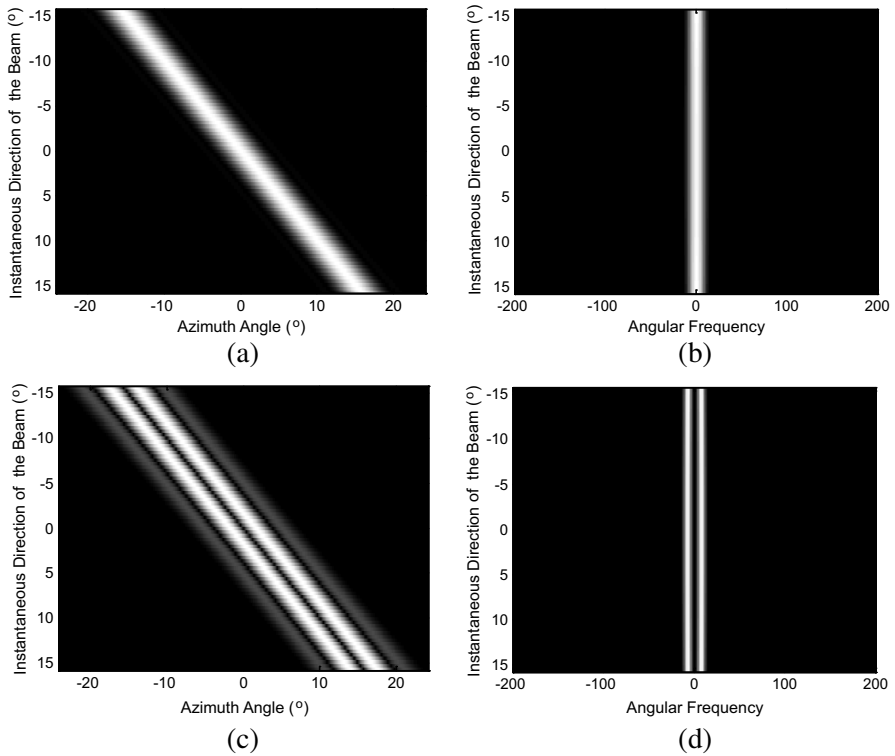Antenna patterns at all the time and these Fourier transformations

Figure 7. Antenna pattern and these spectrums. (a) Antenna patterns of the sum channel. (b) Antenna patterns' spectrums of the sum channel. (c) Antenna patterns of the difference channel. (d) Antenna patterns' spectrums of the difference channel.

are shown in Fig. 7. It shows that bandwidths of the sum channel antenna patterns and the difference channel antenna patterns are extremely limited, therefore, two-channel deconvolution in frequency domain is inefficient when it is used to improve azimuth resolution of the forward-looking image. The reason is that the Fourier transformations of the antenna patterns have a finite bandwidth. In order to overcome this shortcoming, the existing methods use some regularized measurement for deconvolution, such as supposing that the amplitudes of scatterers is positive. However, after pulse compression along the fast time, the amplitudes include the phases which are formed by the fixed distance between the targets and the radar, and these phases cannot be compensated because these positions cannot be obtained accurately enough. It can be seen that these simple regularized measurements are inefficient.

3.2. Analysis of the LSE Forward-looking Imaging Method

If the scanning area is so large that the change of the antenna pattern cannot be ignored, deconvolution method cannot be utilized for forward-looking imaging. So another methods based on the matrix form of the echo which is given by Equations (12) and (13) are proposed, and one of these methods is the LSE, which means that $\mathbf{X}$ is estimated from $\mathbf{S}_\Sigma$ according to the least square criterion. From the above description about the model, we know that the number of unknowns is larger than the number of equations, and LSE can be used to solve the problem and achieved an optimum solution. If the radar is a monopulse one which has two channels, LSE also can be used to image. At this time, $\mathbf{S} = \mathbf{GX} + \mathbf{W}$, where $\mathbf{S} = \begin{bmatrix} \mathbf{S}_\Sigma^T & \mathbf{S}_\Delta^T \end{bmatrix}^T$, $\mathbf{G} = \begin{bmatrix} \mathbf{G}_\Sigma^T & \mathbf{G}_\Delta^T \end{bmatrix}^T$ and the superscript 'T' means transpose operation. As described above, the number of equations will be doubled while the number of unknowns keeps constant, and the number of equations will be larger than that of unknowns. Imaging results of the LSE method can be expressed as

$$\hat{\mathbf{X}} = \left(\mathbf{G}^H\mathbf{G}\right)^{-1}\mathbf{G}^H\mathbf{S} \tag{27}$$

where the superscript 'H' indicates conjugate transpose. Dimension of $\mathbf{G}^H\mathbf{G}$ is $Q \times Q$. Since strong correlations between any two equations may be presented, the rank of $\mathbf{G}$ will be much smaller than the column number, which implies that most of the eigenvalues of $\mathbf{G}^H\mathbf{G}$ are equal to zeros, and $\mathbf{G}^H\mathbf{G}$ is irreversible. In order to eliminate its singularity, Tikhonov regularization method is adopted. And the result of the modified LSE is given by

$$\hat{\mathbf{X}} = \left(\mathbf{G}^H\mathbf{G} + \lambda\mathbf{E}\right)^{-1}\mathbf{G}^H\mathbf{S} \tag{28}$$

where λ is a small positive value, and $\mathbf{E}$ is an identity matrix whose dimension is $Q \times Q$. The singularity is eliminated while the equations are changed significantly and the real solution cannot be achieved. For an instance, if the radar parameters are the same with the above simulation which is used in the last of Section 3.1, the number of scanning steps is 625 from $-15.6°$ to $15.6°$, and the scanning step between two adjacent probes is $0.05°$. The antenna pattern coverage area is from $-15.6 - 8.5 = 24.1°$ to $15.6 + 8.5 = 24.1°$, that is, targets from $-24.1°$ to $24.1°$ are considered. If the sampling interval of the antenna pattern also is $0.05°$, the sampling number of the antenna pattern will be 965, and the number of unknowns is 965. If two channels are used, there will be $625 \times 2 = 1250$ equations. It shows that the number of the equations is larger than that of unknowns. Scatterers' distribution is illustrated in Table 1.

Table 1. Scatterers distribution in the area.

No.	Slant Range/m	Azimuth/°	Amplitude
1	1995	0.5	1
2	1995	0	1
3	1995	−0.5	1
4	2000	0.5	1
5	2000	0	1
6	2000	−0.5	1
7	2005	0.5	1
8	2005	0	1
9	2005	−0.5	1

The condition number of $\mathbf{G}$ which is calculated using Matlab is equal to 1.7944×10^{18}, and the rank of $\mathbf{G}^H \mathbf{G}$ is 30. If $\lambda = 1 \times 10^{-10}$, real beam scanning result and imaging result based on the LSE are shown in Fig. 8. Spots in the figure are the real positions of the scatterers. It shows that the image resolution is improved but the extent is non-significant.

Several simulations validate the conclusion. The reason is that the scanning step is so small that two adjacent rows of $\mathbf{G}_\Sigma$ or $\mathbf{G}_\Delta$ are approximately equal to each other. And the LSE method cannot solve the problem efficiently.

3.3. forward-looking Imaging Based on Compressed Sensing

Above theoretical analysis and numerical simulations show that neither two-channel deconvolution nor the LSE can improve azimuth resolution of the real beam scanning image efficiently. The reason is that in order to solve the inverse problem and improve the azimuth resolution of the image, priori information is essential. If it could be used efficiently, forward-looking imaging with high resolution may be possible. An important priori information is that scattering characteristic of the target area in the optical area is equivalent to the coherent superposition of a number of strong scatterers, these scatterers are only a small part of the area, and amplitudes of the other area are equal to zero approximately. That is to say, the scene is sparse or compressible. Specifically, most of elements of $\mathbf{X}$ are equal to zero, and only few of them have non-zero values, which implies that the inverse problem is a one about sparse signal reconstruction and compressed sensing method could be able to solve the problem. After
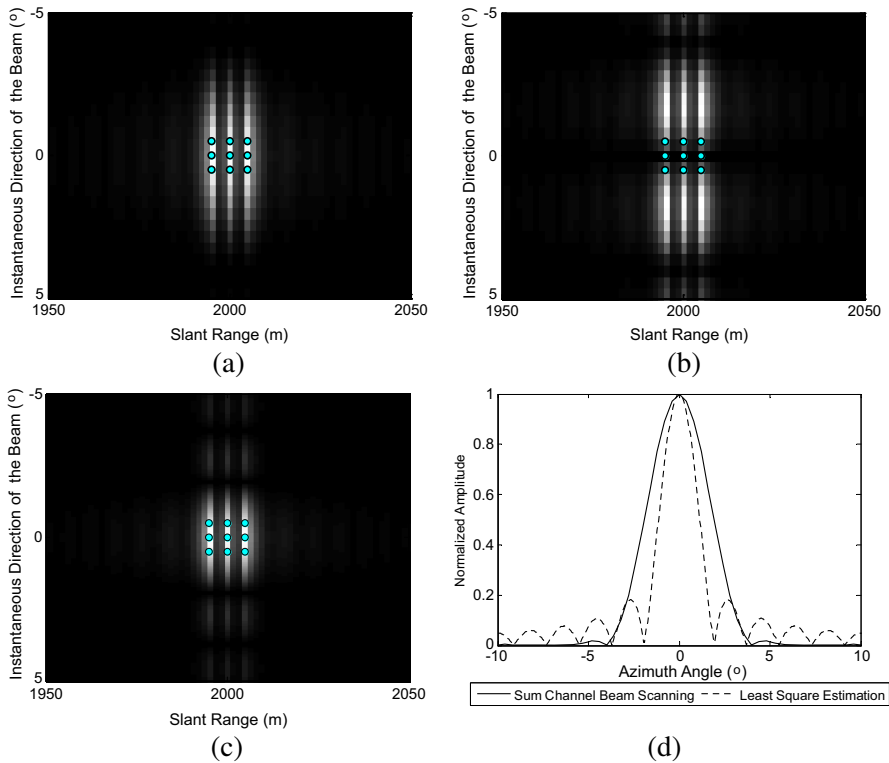
Figure 8. Imaging result of the LSE method. (a) Result of the sum channel. (b) Result of the difference channel. (c) Image by the least square estimation. (d) Azimuth resolution of a target at 2000 m along the slant range.

pulse compression, the u-th column could be abstracted from $\mathbf{S}_\Sigma$ and $\mathbf{X}$, and a novel equation is obtained which is given by

$$\mathbf{s}_u = \mathbf{G}_\Sigma \mathbf{x}_u + \mathbf{w}_u \tag{29}$$

where $\mathbf{w}_u$ indicates the impact of noise, $\mathbf{s}_u$ the u-th column of $\mathbf{S}_\Sigma$, and $\mathbf{x}_u$ the u-th column of $\mathbf{X}$ which indicates the targets' distribution on the u-th isometric ring, and its length is Q. Suppose that there are k scatterers on the ring. Because of the sparsity of the scene, k is much smaller than Q, and $\mathbf{x}_u$ is a sparse vector with the order equal to k. Let $\theta_0 = \theta_0^0 - K\delta\theta$, $\theta_{Q-1} = \theta_{I-1}^0 + K\delta\theta$, $\theta_q = \theta_0 + q\delta\theta$ $(q = 0, 1, \ldots, Q-1)$. Without loss of generality, we can assume that the relationship between the scanning step $\Delta\theta$ and the sampling interval of the antenna pattern $\delta\theta$ is $\Delta\theta = J\delta\theta$, so $\theta_i^0 = \theta_0^0 + i\Delta\theta = \theta_0^0 + iJ\delta\theta$, $i = 0, 1, \ldots, I-1$,

and $\mathbf{G}_\Sigma$ can be expressed as $\mathbf{G}_\Sigma = [\mathbf{g}_{\Sigma 0} \quad \mathbf{g}_{\Sigma 1} \quad \cdots \quad \mathbf{g}_{\Sigma Q-1}]$, where $\mathbf{g}_{\Sigma q} = \left[g_\Sigma \left(\theta_0^0, \theta_q \right) \quad g_\Sigma \left(\theta_1^0, \theta_q \right) \quad \cdots \quad g_\Sigma \left(\theta_{I-1}^0, \theta_q \right) \right]^T$, and in order to bring (29) to a CS scheme, a new vector is constructed which is given by

$$\mathbf{g'}_{\Sigma q} = \left[g_\Sigma \left(\theta_0^0, \theta_q \right), g_\Sigma \left(\theta_0^0 + \delta\theta, \theta_q \right), \ldots, g_\Sigma \left(\theta_0^0 + (J-1)\,\delta\theta, \theta_q \right), \right.$$
$$\left. g_\Sigma \left(\theta_0^0 + J\delta\theta, \theta_q \right), \ldots, g_\Sigma \left(\theta_0^0 + (I-1)\,J\delta\theta, \theta_q \right) \right]^T$$

Thus we have a dense dictionary as follows:

$$\mathbf{G'}_\Sigma = \left[\mathbf{g'}_{\Sigma 0} \quad \mathbf{g'}_{\Sigma 1} \quad \cdots \quad \mathbf{g'}_{\Sigma Q-1} \right]$$

It shows that $\mathbf{G}_\Sigma = \mathbf{D}\mathbf{G'}_\Sigma$, where $\mathbf{D}$ is given by

$$\mathbf{D} = \begin{bmatrix} 1 & 0 & \ldots & 0 & 0 & \ldots & 0 \\ 0 & 0 & \ldots & 1 & 0 & \ldots & 0 \\ \vdots & \vdots & \ddots & \vdots & \vdots & \ddots & \vdots \\ 0 & 0 & \ldots & 0 & 0 & \ldots & 1 \end{bmatrix}$$

Dimension of $\mathbf{D}$ is $I \times [(I-1)J+1]$, only the iJ-th element of the i-th row is equal to 1, and the others are all equal to 0, and that is to say, the matrix $\mathbf{D}$ chooses the columns of $\mathbf{G'}_\Sigma$ whose columns index number is 0, J, iJ, $\ldots$, or $(I-1)J$. So a new equation can be obtained which is written as follows:

$$\mathbf{s}_u = \mathbf{D}\mathbf{G'}_\Sigma \mathbf{x}_u + \mathbf{w}_u = \mathbf{G}_\Sigma \mathbf{x}_u + \mathbf{w}_u \qquad (30)$$

It shows that $\mathbf{s}_u$ is the sparse sampling of $\mathbf{G'}_\Sigma \mathbf{x}_u$ which is impacted by noise. $\mathbf{G}_\Sigma = \mathbf{D}\mathbf{G'}_\Sigma$ is the sparse measurement matrix of a compressed sensing. Forward-looking Imaging based on compressed sensing is to estimate $\mathbf{x}_u$ based on the Equation (30) under the condition that the scene is sparse or compressible. Above analysis shows that $\mathbf{x}_u$ is a sparse representation on the overredundant basis $\{ \mathbf{g}_{\Sigma q} | q = 0, 1, \ldots, Q-1 \}$, where $\mathbf{g}_{\Sigma q}$ is named as an atom. According to the compressed sensing, $\mathbf{x}_u$ can be recovered by solving the following minimization problems which is expressed as:

$$(P_0) \quad \min \|\mathbf{x}_u\|_0 \quad s.t. \|\mathbf{s}_u - \mathbf{G}_\Sigma \mathbf{x}_u\|_2 \le \rho \qquad (31)$$

where, $\|\mathbf{x}\|_0$ indicates the number of non-zero values in the vector, i.e., the sparsity order of the vector. ρ is the error parameter which indicates the impact of noise. Because the minimization is an NP-hard problem, its approximate solution is considered and the minimization problem will be relaxed. It has been verified that under some conditions, the problem can be converted from the nonconvex optimization to a convex one which can be solved using the linear programming technique. And the problem can be relaxed as follows:

$$(P_0) \quad \min \|\mathbf{x}_u\|_1 \quad s.t. \|\mathbf{s}_u - \mathbf{G}_\Sigma \mathbf{x}_u\|_2 \le \rho \qquad (32)$$

Using the famous Laplace method, the problem can be rewritten as

$$\left(P_1^\lambda\right) \quad \hat{\mathbf{x}}_u = \arg\min\left\{\|\mathbf{x}_u\|_1 + \lambda\|\mathbf{s}_u - \mathbf{G}_\Sigma\mathbf{x}_u\|_2\right\} \tag{33}$$

where λ is a positive value, and it is determined by the power of noise. In order to obtain correct reconstruction results, some requirements are placed on the sensing matrix. As mentioned above, one sufficient condition is known as the restricted isometric property (RIP) of the sensing matrix. If the sensing matrix $\mathbf{G}_\Sigma$ satisfies RIP and $I \geq O(k \cdot \log Q)$, $\mathbf{x}_u$ can be recovered exactly with overwhelming probability. A matrix $\mathbf{G}_\Sigma$ is said to satisfy the RIP of order k if there exists a constant $\varepsilon_k \in (0, 1)$ such that

$$(1 - \varepsilon_k)\|\mathbf{x}\|_2^2 \leq \|\mathbf{G}_\Sigma\mathbf{x}\|_2^2 \leq (1 + \varepsilon_k)\|\mathbf{x}\|_2^2 \tag{34}$$

holds for all $\|\mathbf{x}\|_0 \leq k$. ε_k is named as restricted isometric constant (RIC). If the sensing matrix satisfies the RIP with appropriate order and constant, the solution of the (P_1) problem in Equation (31) will be equivalent to that of the (P_0) problem in Equation (32), and the (P_1^λ) problem can also recover sparse signal in noise stably. RIP is broadly viewed as a sufficient criterion for evaluating whether a dictionary behaves like an isometry system in CS recovery. However, for a special dictionary, in general, it is not easy to test whether $\mathbf{G}_\Sigma$ satisfies RIP. Herein, a method based on eigenvalue statistics which has been described in [46] is adopted. After scaling, columns of $\mathbf{G}_\Sigma$ have unit norm, and it is explicit that $\mathbf{G}_\Sigma$ obeys-the RIP of order k when $\mathbf{G}_{\Sigma k}^T\mathbf{G}_{\Sigma k}$ has eigenvalues sufficiently within $(1 - \delta_k, 1 + \delta_k)$. Herein, $\mathbf{G}_{\Sigma k}$ is constructed by abstracting k columns from the scaled $\mathbf{G}_\Sigma$, and the index number of columns are random, so there will be many sets. Each set will have its own maximum eigenvalue $e_{k\max}$ and minimum eigenvalue $e_{k\min}$. The means of $e_{k\max}$ and $e_{k\min}$ can be obtained which are denoted as $\hat{e}_{k\max}$ and $\hat{e}_{k\min}$. If $\hat{e}_{k\max}$ and $\hat{e}_{k\min}$ are all within $(1 - \varepsilon_k, 1 + \varepsilon_k)$, we can speculate that $\mathbf{G}_\Sigma$ satisfies the RIP of order k. In the experiment, supposing that the radar scans from $-15.6°$ to $15.6°$ with a uniform step, coverage of the scanning processing ranges from $-24.1°$ to $24.1°$. The sampling interval of the antenna pattern is $0.05°$, and the number of the sampling points is 965, and spacing between two adjacent elements keeps 0.6 times of the wavelength. k varies from 1 to 30. Fig. 9(a) shows the means of the maximum and the minimum eigenvalues of $\mathbf{G}_\Sigma$ with $M_x = 25, 35, 45, 55$. Fig. 9(b) shows the means of the maximum and the minimum eigenvalues of $\mathbf{G}_\Sigma$ if there are $I = 40, 79, 157, 313, 625$ samplings available.

Some conclusions can be deduced from above experiment:

(1) Under the condition that $M_x = 25$, the means of the maximum and the minimum eigenvalues are within (0, 2) only when the
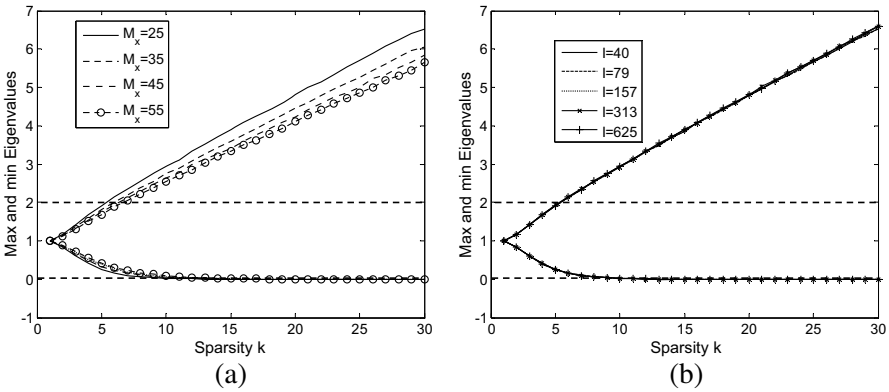
Figure 9. Analyzing RIP of $\mathbf{G}_\Sigma$. (a) Relationship between RIC and M_x. (b) Relationship between RIC and sampling number.

order of sparsity k is less than 5, which indicates that there exists a positive value $\varepsilon_k \in (0, 1)$. RIP is satisfied and the sparse vector can be recovered exactly by solving the optimum problem. But if $k > 5$, the mean of these maximum eigenvalues will be larger than two, RIP cannot be satisfied, and the problem cannot be solved by the convex optimization. In order to overcome this difficulty, performance of the sensing matrix $\mathbf{G}_\Sigma$ should be improved through some methods, such as more complicated antenna pattern design.

(2) If M_x increases and the sparsity order of the vector keeps constant, RIC will decrease and $\mathbf{x}_u$ will be recovered more easily. This is consistent with the intuition. More elements mean a narrower beam width and better azimuth resolution. But the cost, volume and weight of the radar will increase.

(3) Under the condition that $I \geq O(k \cdot \log Q)$, the maximum and minimum eigenvalues do not change with the number of the scanning steps, which is shown in Fig. 9(c) and indicates that we can obtain the high azimuth resolution with the fewest number of scanning steps.

In summary, the proposed forward-looking imaging method based on compressed sensing includes the following steps:

(1) A train of pulses with a large time-bandwidth product are emitted to the target area which is located at the front of the monopulse PAR at the same time the radar is scanning along the azimuth direction, and echoes are collected by the radar.

(2) High range resolution profiles are obtained after pulse compression to echoes of each pulse.

(3) Echoes in each range cell from the sum channel is used to estimate the distribution of the scatterers based on compressed sensing respectively, and the azimuth discrimination is achieved.

4. SIMULATION RESULTS

In order to validate the proposed method and compare it with the imaging results of the real beam scanning and the LSE method, some simulations' results are presented. Herein, point scattering model is used. Since the imaging in three dimensional space is equivalent to the imaging in the two dimensional space which is determined by the spindle of the beam, these simulations are performed in the two-dimensional space. Parameters used in the simulations are given below: the operating frequency is 35 GHz, the space between two adjacent elements is 0.6 times of the wavelength, and there exists 25 elements in the array. The beam scans from $-15.6°$ to $15.6°$, the number of the scanning steps is 79, and the scanning step is $0.4°$. The target area locates at the front of the radar from $-24.1°$ to $24.1°$. Chirp pulses are transmitted, and the instantaneous bandwidth is equal to 80 MHz, which means that the range resolution is 1.875 meters. Three simulations are carried out as follows.

4.1. Validity Simulation

In order to validate the method, suppose that there are nine scatterers in the target area and that their polar coordinates are [1995 m, $0.4°$], [1995 m, $0°$], [1995 m, $-0.4°$], [2000 m, $0.4°$], [2000 m, $0°$], [2000 m, $-0.4°$], [2005 m, $0.4°$], [2005 m, $0°$], and [2005 m, $-0.4°$], respectively. Amplitudes of the scatterers are all uniform. Noise impact is ignored. Figs. 10(a) and (b) show the imaging results of the target area based on the real beam scanning and the LSE method. Spots in the figures are the real positions of the scatterers. It can be seen that neither of them can discriminate two adjacent scatterers in the same range resolution cell. Fig. 10(c) shows the imaging result of the proposed method. Compared with above figures, it can be seen that the azimuth resolution is improved significantly, and the scatterers can be discriminated easily. Fig. 10(d) shows the imaging results of the scatterers whose range are 2000 meters, which indicates that azimuth resolution based on the LSE method is better than that of the real beam scanning, but cannot discriminate two adjacent scatterers, and azimuth resolution based on compressed sensing is the best. Validation of the method is verified.
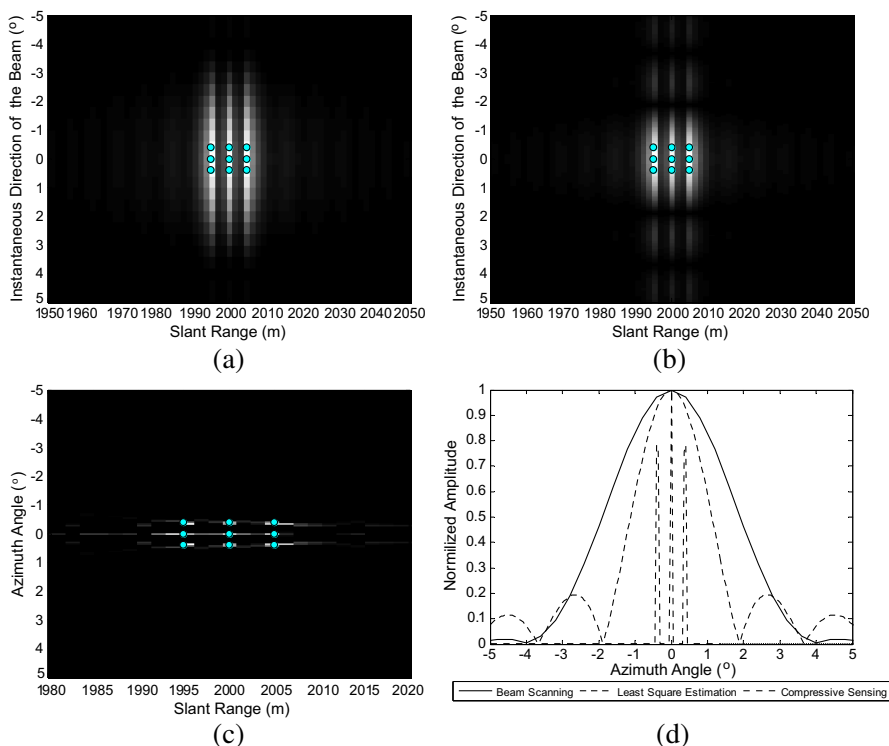
Figure 10. Efficiency of the imaging method by the compressive sensing. (a) Scanning result of the sum channel. (b) Imaging result after the least square estimation. (c) Imaging result of the compressive sensing method. (d) Results' comparison of different methods.

4.2. Robustness Test

To verify the robustness of the algorithm, we designed the following experiment: radar operating parameters have been mentioned above, and assuming there is a scatterer whose range is 2000 meters and azimuth angle is $-0.5°$. Gaussian white noise model is assumed, and Monte Carlo experiments are carried out and the signal-to-noise ratio (SNR) ranges from 0 dB to 45 dB. Five hundred experiments are carried out under each SNR. Herein, the SNR is defined as the ratio of the echo's total energy to noise power, which is given by

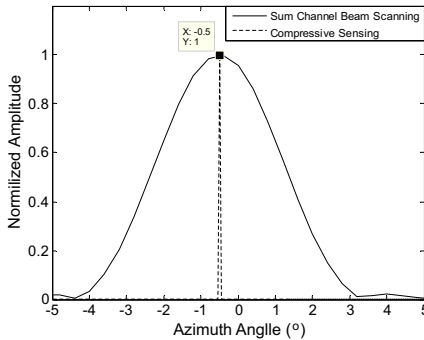$$SNR = 10 \log_{10} \frac{\mathbf{s}_u^H \mathbf{s}_u / I}{\sigma^2}$$

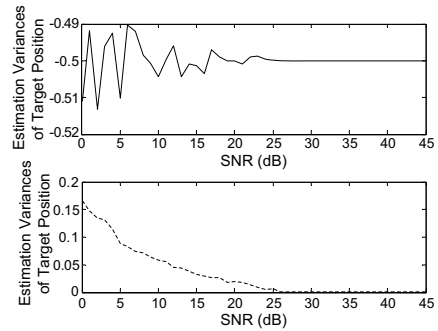**Figure 11.** Image of beam scanning and compressive sensing.

Figure 12. Estimation means and variance of compressive sensing under different SNRs.

Figure 11 shows the imaging results along azimuth dimension based on the real beam scanning and the compressed sensing. Herein, noise impact is not considered. It indicates that azimuth resolution of the proposed method is better. Since the target occupies only one or two points and it is difficult to define the azimuth resolution of the imaging result, the mean and variance of the optimum estimation are selected as a measure of imaging result.

It shows that even at low SNR, high azimuth resolution can be achieved. However, it should be noted that lower SNR means longer time for estimation. Fig. 12 shows the change rules of the mean and variance via the SNR, which indicates that if the SNR increases, estimation of the target position will be more accurate and the variance of the estimation will be lower. It can be seen that improvement of the SNR is benefit for estimation.

4.3. Impact Analysis of RIC

If the elements' number M_x keeps constant, a greater order of sparsity k means a larger RIC. And if the order of sparsity k keeps constant, a greater M_x means a smaller RIC. Supposing that $M_x = 25$ and noise does not exist, imaging results are illustrated in Fig. 13 with $k = 2, 3, 4$. Herein, the azimuth angle interval between two adjacent scatterers is $0.4°$. It shows that the correct recovery can be achieved if $k < 4$. Otherwise, we cannot achieve the correct recovery.

If k keeps constant which is equal to 3 and the azimuth angle interval between two adjacent scatterers is $0.3°$, imaging results are given in Fig. 14 with $M_x = 25, 35, 45$. It shows that if M_x increase, results of the estimation will be better. So a conclusion can be achieved
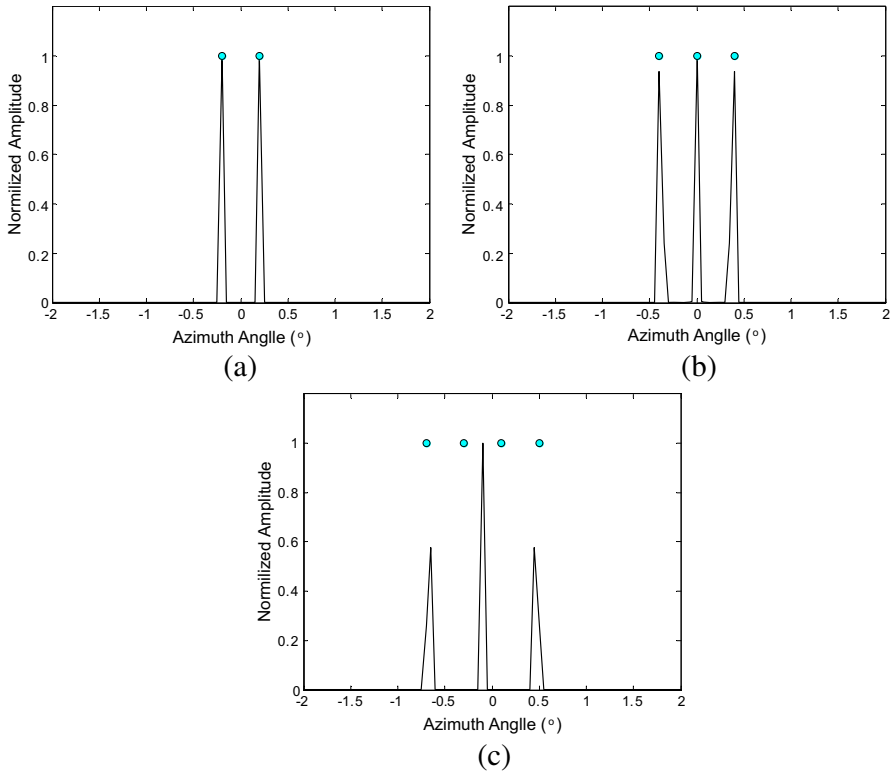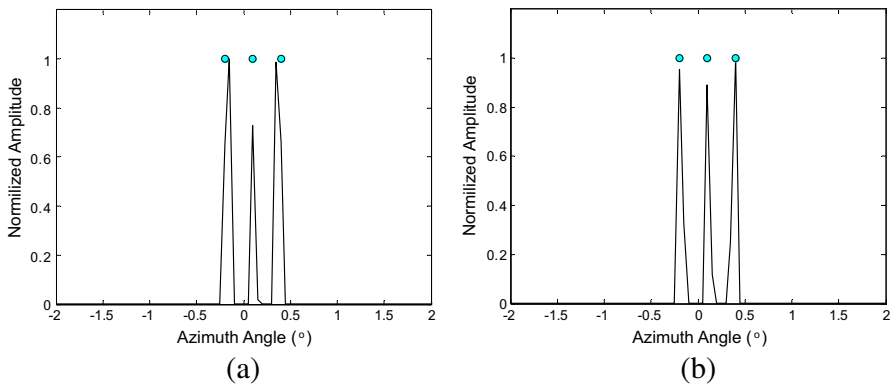
Figure 13. Relationship between the estimation result and the scatterers' number. (a) $k = 2$. (b) $k = 3$. (c) $k = 4$.
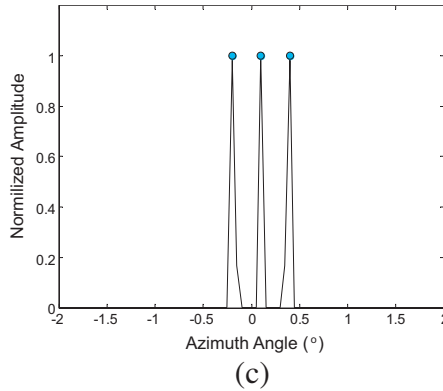
(c)

Figure 14. Relationship bet the estimation result and the elements number. (a) $M_x = 25$. (b) $M_x = 35$. (c) $M_x = 45$.

that RIC is important for the forward-looking imaging based on the compressed sensing. In order to obtain smaller RIC, the number of elements in the array should be increased, but the cost increases dramatically, and a comprise needs to be done.

5. CONCLUSION

In order to improve the azimuth resolution of the image based on the real beam scanning under the forward-looking condition, a novel method based on the compressed sensing is proposed. Simulations verify the method and images with high resolution are achieved under certain conditions. The algorithm does not require a large antenna aperture or large-scale transformation, especially, relative tangential motion between targets and the radar. The azimuth resolution can be improved through signal processing, which should be a promising method for forward-looking imaging.

REFERENCES

1. Berens, Dr., P., "Introduction to synthetic aperture radar (SAR)," *Advanced Radar Signal and Data Processing*, RTO-EN-SET-086, 3-1–3-14, 2006.
2. Ouchi, K., "Recent trend and advance of synthetic aperture radar with selected topics," *Remote Sensing*, No. 5, 716–807, 2013.
3. Sun, J. P., Y. X. Zhang, J. H. Tian, et al., "A novel spaceborne SAR wide-swath imaging approach based on poisson disk-like

nonuniform sampling and compressive sensing," *Science China*, Vol. 55, No. 8, 1876–1887, August 2012.

4. Palash, J. and K. R. Sarma, "Azimuth triangulation method for forward looking synthetic aperture radar," *International Journal on Recent and Innovation Trends in Computing and Communication*, Vol. 1, No. 3, 106–109, March 2013.

5. An, D. X., X. T. Huang, T. Jin, et al., "Extended nonlinear chirp scaling algorithm for high-resolution highly squint SAR data focusing," *IEEE Trans. on Geosci. Remote Sens.*, Vol. 50, No. 9, 3595–3609, September 2012.

6. Nam, S., J. S. Lee, and J. S. Ha, "Antenna aperture design scheme for the bistatic forward looking SAR application," *IEEE the 3rd International Asia-Pacific Conference on Synthetic Aperture Radar (APSAR)*, 1–4, September 2011.

7. Witte, F., T. Sutor, and R. Scheunemann, "A new sector imaging radar for enhanced vision — SIREV," *Proceedings of the SPIE Conference in Enhanced and Synthetic Vision*, Vol. 3364, 115–122, April 1998.

8. Sutor, T., S. Buckreuss, G. Krieger, et al., "Sector imaging radar for enhanced vision (SIREV): Theory and applications," *Proceedings of SPIE in Enhanced and Synthetic Vision*, Vol. 4023, 292–297, June 2000.

9. Mittermayer, J., M. Wendler, G. Krieger, et al., "Sector imaging radar for enhanced vision (SIREV): Simulation and processing techniques," *Proceedings of SPIE in Enhanced and Synthetic Vision*, Vol. 4023, 298–305, June 2000.

10. Krieger, G., J. Mittermayer, M. Wendler, et l., "SIREV-sector imaging radar for enhanced vision," *Proceedings of the 2nd International Symposium in Image and Signal Processing and Analysis*, 377–382, 2001.

11. Ren, X. Z., J. T. Sun, and R. L. Yang, "A new three-dimensional imaging algorithm for airborne forward-looking SAR," *IEEE Geosci. Remote Sens. Letts.*, Vol. 8, No. 1, 153–157, January 2011.

12. Purik, D., S. H. Han, S.-G. Sun, et al., "2D frequency domain imaging algorithms for forward looking array radar," *Proceedings of the 9th European Radar Conference*, 22–25, Amsterdam, The Netherlands, October 2012.

13. Mahafza, B. R., D. L. Knight, and N. F. Audeh, "Forward-looking SAR imaging using a linear array with transverse motion," *IEEE Proceedings in Southeastcon*, 4–7, April 1993.

14. Xiang, G., X. L. Zhang, J. Shi, et al., "Airborne 3-D forward looking SAR imaging via chirp scaling algorithm," *Geoscience and Remote Sensing IEEE International Symposium — IGARSS*, 3011–3014, July 2011.

15. Peng, X., W. Tan, Y. Wang, W. Hong, and Y. Wu, "Convolution back-projection imaging algorithm for downward-looking sparse linear array three dimensional synthetic aperture radar," *Progress In Electromagnetics Research*, Vol. 129, 287–313, 2012.

16. Sun, S. G., G. C. Park, B. L. Choe, et al., "Forward-looking 3D imaging radar and method for acquiring 3D images using the same," US Patent Application, Patent No: US 8471759 B2, June 25, 2013.

17. Zheng, Y. B., S.-M. Tseng, and K.-B. Yu, "Closed-form four-channel monopulse two-target resolution," *IEEE Trans. on Aero. Elec. Syst.*, Vol. 39, No. 3, 1083–1089, July 2003.

18. Stimson, G. W., *Introduction to Airborne Radar*, SciTech Pub., 1998.

19. Liu, G. Q., K. Yang, B. Sykora, et al., "Range and azimuth resolution enhancement for 94 GHz real-beam radar," *Proceedings of SPIE on Radar Sensor Technology XII*, Vol. 6947, 1–9, 2008.

20. Bouchard, C. and D. Grenier, Dr., "ISAR imaging radar with time-domain high-range resolution algorithms and array antenna," Laboratoire de Radiocommunications et de Traitement du Signal, Raport Annuel, 1997–1998.

21. Deng, W. B. and Z. Bao, "Radar imaging based on rotating antenna," *1988 International Conference on Acoustics, Speech, and Signal Processing, ICASSP-88*, Vol. 2, 1196–1199, New York, NY, April 1988.

22. Li, W., J. Yang, and Y. Huang, "Keystone transform-based space-variant range migration correction for airborne forward-looking scanning radar," *Electronics Letters*, Vol. 48, No. 2, 121–122, January 2012.

23. Browne, K. E., R. J. Burkholder, and J. L. Volakis, "A novel low-profile portable radar system for high resolution through-wall radar imaging," *2010 IEEE Radar Conference*, 333–338, Washington DC, May 2010.

24. Berenstein, C. A. and E. V. Partick, "Exact deconvolution for multiple convolution operators — An overview, plus performance characterizations for imaging sensors," *Proceedings of the IEEE*, Vol. 78, No. 4, 723–734, April 1990.

25. Richards, M. A., "Iterative noncoherent angular superresolution," *Proceedings of the 1988 IEEE National Radar Conference*, 100–105, Ann Arbor, MI, April 1988.

26. Suwa, K. and M. Iwamoto, "Forward looking radar imaging method using multiple receiver antennas and digital beam forming technique," *Proceedings. 2005 IEEE Geoscience and Remote Sensing Symposium, IGARSS'05*, Vol. 6, 4041–4044, July 2005.

27. Ruggiano, M., E. Stolp, and V. Genderen, "Improvement of target resolution in azimuth by LMMSE technique," *2009 European Radar Conference*, 230–233, Rome, September 2009.

28. McIntosh, J. C., A. Kennedy, and C. Clary, "Scanned time/angle correlation: A new method for super-resolution," *Proceedings of SPIE on Algorithms for Synthetic Aperture Radar Imagery XII*, Vol. 5808, 95–101, Bellingham, WA, 2005.

29. Sun, J., S. Mao, and G. Wang, "Polar format algorithm for spotlight bistatic SAR with arbitrary geometry configuration," *Progress In Electromagnetics Research*, Vol. 103, 323–338, 2010.

30. Wu, J., Z. Li, Y. Huang, Q. H. Liu, and J. Yang, "Processing one-stationary bistatic SAR data using inverse scaled fourier transform," *Progress In Electromagnetics Research*, Vol. 129, 143–159, 2012.

31. Espeter, T., I. Walterscheid, J. Klare, et al., "Bistatic forward-looking SAR: Results of a spaceborne-airborne experiment," *IEEE Trans. on Geosci. Remote Sens. Letts.*, Vol. 8, No. 4, 765–768, July 2011.

32. Wu, J. J., Z. Y. Li, Y. L. Huang, et al., "Focusing bistatic forward-looking SAR with stationary transmitter based on keystone transform and nonlinear chirp scaling," *IEEE Geosci. Remote Sens. Letts.*, Vol. PP, No. 99, May 2013.

33. Li, W. C., Y. L. Huang, J. Y. Yang, et al., "An improved radon-transform-based scheme of doppler centroid estimation for bistatic forward-looking SAR," *IEEE Geosci. Remote Sens. Letts.*, Vol. 8, No. 2, 379–383, March 2011.

34. Shin, H.-S. and J.-T. Lim, "Omega-k algorithm for airborne forward-looking bistatic spotlight SAR imaging," *IEEE Geosci. Remote Sens. Letts.*, Vol. 6, No. 2, 312–316, April 2009.

35. Walterscheid, I., T. Espeter, J. Klare, et al., "Potential and limitations of forward-looking bistatic SAR," *2010 IEEE International Geoscience and Remote Sensing Symposium (IGARSS)*, 216–219, Honolulu, HI, July 2010.

36. Walterscheid, I., A. R. Brenner, and J. Klare, "Radar imaging with very low grazing angles in a bistatic forward-looking configuration," *2012 IEEE International Geoscience and Remote Sensing Symposium (IGARSS)*, 327–330, Munich, July 2012.

37. Qiu, X. L., D. H. Hu, and C. B. Ding, "Some reflections on bistatic SAR of forward-looking configuration," *IEEE Geosci. Remote Sens. Letts.*, Vol. 5, No. 4, 735–739, October 2008.

38. Nguyen, N., P. Milanfar, and G. Golub, "A computationally efficient superresolution image reconstruction algorithm," *IEEE Trans. on Image Proc.*, Vol. 10, No. 4, 573–583, April 2001.

39. Vogel, C. R. and M. E. Oman, "Fast, robust total variation-based reconstruction of noisy, blurred images," *IEEE Trans. on Image Proc.*, Vol. 7, No. 6, 813–824, June 1998.

40. Candès, E. J. and M. B. Wakin, "An introduction to compressive sampling," *IEEE Signal Processing Magazine*, Vol. 25, No. 2, 21–30, March 2008.

41. Patel, V. M., G. R. Easley, D. M. Healy, et al., "Compressed synthetic aperture radar," *IEEE Journal of Selected Topics in Signal Processing*, Vol. 4, No. 2, 244–254, April 2010.

42. Fang, J., Z. B. Xu, B. C. Zhang, et al., "Fast compressed sensing SAR imaging based on approximated observation," *IEEE Journal of Selected Topics in Applied Earth Observations and Remote Sensing*, Vol. PP, No. 99, 1–12, May 2013.

43. Alonson, M. T., P. Lopez-Dekker, and J. J. Mallorqui, "A novel strategy for radar imaging based on compressive sensing," *IEEE Trans. on Geosci. Remote Sens.*, Vol. 49, No. 12, 4285–4295, December 2012.

44. Qu, Y., G. Liao, S.-Q. Zhu, and X.-Y. Liu, "Pattern synthesis of planar antenna array via convex optimization for airborne forward looking radar," *Progress In Electromagnetics Research*, Vol. 84, 1–10, 2008.

45. Mailloux, R. J., *Phased Array Radar*, 2nd Edition, Artech House, 2005.

46. Zhang, L., M. D. Xing, C. W. Wiu, et al., "Resolution enhancement for inversed synthetic aperture radar imaging under low snr via improved compressive sensing," *IEEE Trans. on Geosci. Remote Sens.*, Vol. 48, No. 10, 3824–3838, October 2010.